A Novel Porous-Dense Dual-Layer Composite Membrane Reactor with Long-Term Stability

Wei Jiang, Guangru Zhang, Zhengkun Liu, Kai Zhang, and Wanqin Jin
State Key Laboratory of Materials-Oriented Chemical Engineering, College of Chemistry and Chemical engineering, Nanjing University of Technology, 5 Xinmofan Road, Nanjing 210009, P. R. China

DOI 10.1002/aic.14178
Published online July 12, 2013 in Wiley Online Library (wileyonlinelibrary.com)

A porous-dense dual-layer composite membrane reactor was proposed. The dual-layer composite membrane composed of dense 0.5 wt % Nb_2O_5-doped $SrCo_{0.8}Fe_{0.2}O_{3-\delta}$ (SCFNb) layer and porous $Ba_{0.3}Sr_{0.7}Fe_{0.9}Mo_{0.1}O_{3-\delta}$ (BSFM) layer was prepared. The stability of SCFNb membrane reactor was improved significantly by the porous-dense dual-layer design philosophy. The porous BSFM surface-coating layer can effectively reduce the corrosion of the reducing atmosphere to the membrane, whereas the dense SCFNb layer permeated oxygen effectively. Compared with single-layer dense SCFNb membrane reactor, no degradation of performance was observed in the dual-layer membrane reactor under partial oxidation of methane during continuously operating for 1500 h at 850°C. At 900°C, oxygen flux of 18.6 mL (STP: Standard Temperature and Pressure) cm^{-2} min^{-1}, hydrogen production of 53.67 mL (STP) cm^{-2} min^{-1}, CH_4 conversion of 99.34% and CO selectivity of about 94% were achieved. *AIChE J*, 59: 4355–4363, 2013
Keywords: oxygen permeation, composite membrane, partial oxidation of methane, hydrogen production, long-term operation

Introduction

In recent years, membrane reactors have attracted considerable attention from scientists and engineerings in chemical and biochemical engineering due to the possibility in coupling the chemical reaction and the separation of feed compenents and/or reaction products in one unit.[1–3] Dense mixed ion-electronic conducting (MIEC) materials, with great oxygen ionic and electronic conductivities at high temperatures have attracted considerable interests in many applications such as effective utilization of natural gas[4–13] or coke oven gas,[14,15] production of hydrogen,[16–18] selective oxidation of light hydrocarbons to high-added-value-chemicals[19–22], and treatment of atmospheric pollutants, expecially CO_2 and NO_X.[11,23–25] MIEC membrane reactors can overcome many of the shortcomings of conventional packed-bed reactors. For example, it controls distribution of oxygen and improves the selectivity or heat-distribution in the reaction side under partial oxidation of methane (POM).[26,27] For potential industrial applications of MIEC membrane reactors, two properties are crucial. First of all, it should be able to sustain a certain oxygen flux. Second, it must be sufficiently stable to allow long-term operation at the relevant operating conditions, particularly in reducing gas atmospheres or atmospheres containing CO_2, SO_2, or H_2O. Unfortunately, few MIEC membrane reactors with high oxygen flux are able to tolerate these environments for long time.[28]

In the past decades, most researches are focused on single-layer membrane reactors where the membrane materials are the critical component. Normally, cobalt-containing membrane materials possess high oxygen permeability but low chemical stability, such as $SrCo_{0.8}Fe_{0.2}O_{3-\delta}$ (SCF) membrane which cracked into several pieces after passing a methane stream through the membrane surface.[29] Moreover, the surfaces of $Ba(Co_xFe_yM_{1-x-y})O_{3-\delta}$ (M = Nb, Ta, Zr) decomposed when they were used for partial oxidation of methane in coke oven gas, POM, and coupling of water splitting with the dehydrogenation of ethane.[15,30,31] Some other membrane materials in which the reducible ions (Co^{n+}, Fe^{n+}) were partially substituted by ions with constant valence (Zr^{4+}, Nb^{5+}, Ga^{3+}, Al^{3+})[32–35] have been developed. Besides, stable oxides such as (Al_2O_3, $SrAl_2O_4$)[36,37] have been used to improve the stability of the membrane materials for membrane reactors. Even several cobalt-free perovskite membranes materials such as $SrAl_xFe_{1-x}O_{3-\delta}$,[38] $La_{0.4}Ba_{0.6}Fe_{0.8}Zn_{0.2}O_{3-\delta}$[39] were reported. The improvement of chemical stability was achieved. However, the oxygen permeation fluxes could rarely reach the level of cobalt-containing materials due to the relatively low oxygen permeability.

In addition to single-phase membranes, dual-phase membranes consist of electronic conducting materials and oxygen ionic conducting materials have been investigated in single-layer membrane reactors extensively. For example, dual-phase membranes based on $Ce_{0.8}Sm_{0.2}O_{1.9}$-$Sm_{1-x}Ca_xMn_{0.5}Co_{0.5}O_3$ ($x = 0$ or $x = 0.2$),[40] 40 wt % $Pr_{0.6}Sr_{0.4}FeO_{3-\delta}$−60 wt % $Ce_{0.9}Pr_{0.1}O_{2-\delta}$,[41] $Zr_{0.84}Y_{0.16}O_{1.92}$-$La_{0.8}Sr_{0.2}Cr_{0.5}Fe_{0.2}O_{3-\delta}$,[42] and 75 wt % $Ce_{0.85}Sm_{0.15}O_{1.95}$−25 wt % $Sm_{0.6}Sr_{0.4}FeO_{3-\delta}$[43] have been used in membrane reactors which contained CO_2 or reducing atmosphere. Generally, the stability of dual-phase

Correspondence concerning this article should be addressed to W. Jin at wqjin@njut.edu.cn.

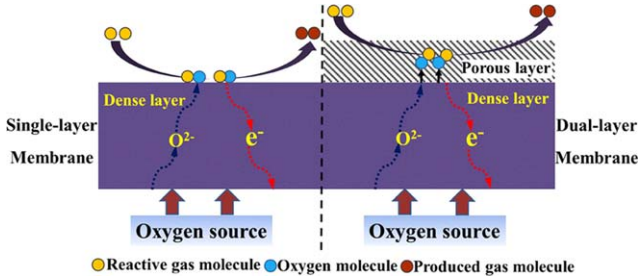

Figure 1. Schematic diagram of a porous-dense dual-layer composite membrane.

[Color figure can be viewed in the online issue, which is available at wileyonlinelibrary.com.]

membranes have been improved, nevertheless, the oxygen permeability is relatively low. For economical attractiveness, Bredense and Sogge[44] reported that an oxygen flux of 10 mL cm^{-2} min^{-1} is needed for syngas production. However, few MIEC membrane reactors could meet the requirement.

According to recent study, due to the issues of stability and permeability, we have to notice that it is difficult for those materials to be independently used in the membrane reactors, especially for multireaction system. A trade-off between high oxygen permeation and good stability was found in single-layer membranes that suffer from the erosion when they were developed to conduct oxygen ions effectively. In our previous experiment, we have used varied single-layer membrane reactors for POM,[8,36,37] oxidative stream reforming of methane,[27] thermal decomposition of CO_2,[23,45] decomposition of CO_2 coupled with POM,[46] and bio-ethanol oxidative steam reforming coupled with water splitting.[18] However, these applications for membrane reactors involved the contacting of membrane surface with reacting environments such as reducing or carbon-rich atmospheres. There is a great challenge for single-layer membrane reactors to obtain the balance between high oxygen permeability and sufficient chemical stability. Also, we have developed asymmetric membrane structure which slowed the erosion of the atmosphere in some way. Nevertheless, it still suffered from the same problems with singer-layer membranes.[47]

The present study aims to develop a porous-dense dual-layer composite membrane reactor where the composite membrane is composed of two close contact layers with different functions. As shown in Figure 1, the dense layer which made of high oxygen ions-conducting materials is mainly for oxygen permeation. The porous layer which consists of good reduction-tolerant materials is mainly for reducing the erosion of reacting atmospheres. The dual-layer composite membranes are expected to play their respective functions and combine the advantages of each layer. The two materials referred to this article 0.5 wt % Nb_2O_5-doped $SrCo_{0.8}Fe_{0.2}O_{3-\delta}$ (SCFNb),[48] $Ba_{0.3}Sr_{0.7}Fe_{0.9}Mo_{0.1}O_{3-\delta}$ (BSFM)[49] have been developed in our experiment recently. They have been proved to own superiorities of good oxygen permeability and high chemical stability. On the base of the porous-dense dual-layer composite membrane (BSFM-SCFNb), we also designed the BSFM-SCFNb porous-dense dual-layer composite membrane reactor for POM to investigate its performance.

Experimental Section

Powder and membrane preparation

The SCF and BSFM powders were synthesized via a combined ethylenediaminetetraacetic acid (EDTA)–citrates complexing sol-gel process with Ba, Sr, Co, and Fe metal nitrates and MoO_3 (dissolved in $NH_3{\cdot}H_2O$ first). Stoichiometric amounts of nitrates were mixed into a certain amount of deionized water under continuous agitation. The necessary amount of EDTA dissolved in $NH_3{\cdot}H_2O$, was then dropped to the mixed metal nitrate solution, followed by the addition of solid citric acid with stirring (mole ration of total metal ions to EDTA and to citrate = 1:1:2). $NH_3{\cdot}H_2O$ was added to adjust the pH value to 6–7 to obtain a clear solution. The solution containing the complex precursor was heated on a hot plate at 250°C for about 5 h with a combustion reaction to produce a gel. Finally, the products were calcined in air at 950°C for 5 h.

SCFNb powders were prepared by mixing 0.5 wt % of Nb_2O_5 with SCF powders (ball-milled in ethanol for 24 h) and calcined in air at 950°C for 5 h. The powders were uniaxially pressed at 4 MPa to prepare the green disk members with the diameter of 16 mm. The members were then sintered in a furnace at 1200°C for 5 h to form the dense bodies.

After polished to a thickness of 1.0 mm with 2000-mesh abrasive papers, the dense SCFNb membrane was sprayed with a BSFM porous layer on methane side. A slurry of 8.41 wt % of BSFM powders, 6.43 wt % glycerin, 18.91 wt % ethylene glycol, and 66.25 wt % isopropyl alcohol was used as spraying fluid. The BSFM-SCFNb membrane was prepared by spraying method, whose detailed description was reported in our previous work.[50] First, the dense SCFNb membrane was placed on a heating platform and the temperature of the heating platform was controlled at 250°C. Then, the slurry was sprayed on the dense SCFNb membrane at a rate of 2.2 mL min^{-1} by using a spraying gun. Finally, with the evaporation of organics, the BSFM powders were deposited on the SCFNb membrane. The coated sample was dried then heated at 1000°C for 2 h with heating and cooling rate of 2°C/min. The average particle size of BSFM was about 260 nm. An uniform coating layer could be formed on the surface of the dense SCFNb membrane. The BSFM-SCFNb dual-layer composite membrane was successfully prepared with a dense SCFNb layer and a porous BSFM layer. The thicknesses of both layers were 1.0 mm and 20 μm, respectively.

Characterization

The particle size of powders was examined by zetatrac analyzer (Microtrac company). The crystal structures of the samples were characterized by X-Ray Diffraction (XRD, ARL X'TRA diffractometer) with Cu Kα radiation in air. The experimental diffraction patterns were collected at room temperature by step scanning in the range $20° \leq 2\theta \leq 80°$ with an increment of 0.05°. The morphologies of sintered membranes were examined by scanning electron microscopy (SEM) (Hitachi S-4800, Japan). The elements of the samples were analyzed by energy dispersive x-ray detector (HORIBA EMAX). Oxygen temperature-programmed desorption (O_2-TPD) experiment was carried out on a conventional apparatus equipped with a mass spectrometer (AMETEK, LCD-200) to investigate the carbon deposition of the catalyst.

Membrane reactor set-up

The reactor module for membrane reaction experiment is illustrated in Figure 2. A prepared membrane disk was mounted on a quartz tube with 6 mm ID (Inner Diameter)

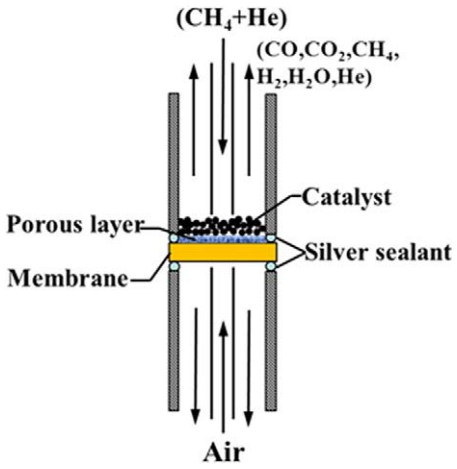

Figure 2. Illustration of the reactor module.

[Color figure can be viewed in the online issue, which is available at wileyonlinelibrary.com.]

and 12 mm OD (Outer Diameter). We used silver as a seal that owns low and negligible oxygen permeation flux due to the poor oxygen ion conductivity.[51,52] 0.1-g 20–40 mesh Ni/Al_2O_3 catalyst was directly loaded on the membrane. Dried synthesized air (O_2, 21%) was introduced into the lower chamber, whereas high purity CH_4 (diluted by He) was introduced into the upper chamber. Both upper and lower chambers were maintained at the atmospheric pressure. The gas flow rates were controlled by mass flow controller (Model AI-708PA, Xiamen Yudian automation technology Co.,). The effluent streams were analyzed by two online gas chromatographs (GC, Shimadzu, model GC-8A, Japan) equipped with a 5A molecule sieve column and a TDX-01 column. The analyses were checked by the carbon balance, which was within 1% for all reaction experiments and could be neligible. We also conducted the O_2-TPD experiment on the used catalyst after the long-term operation. The percentage of the carbon deposition was about 0.25% and could be also negligible. So, we thought that there was hardly carbon deposited on the catalyst in the reaction process.

The oxygen permeation fluxes through the membranes were calculated from the effluent flow rate and the concentration of oxygen-containing compounds in the effluent. The oxygen permeation flux, selectivity, and conversion for POM were calculated using the following equations

$$X_{CH_4} = \frac{F_{CH_{4,inlet}} - F_{CH_{4,outlet}}}{F_{CH_{4,inlet}}} \quad (1)$$

$$S_{CO} = \frac{F_{CO}}{F_{CH_{4,inlet}} - F_{CH_{4,outlet}}} \quad (2)$$

$$F_{O_{2,inlet}} = F_{O_{2,outlet}} + \frac{1}{2}F_{CO} + F_{CO_2} + \frac{1}{2}F_{H_2O} \quad (3)$$

where X_{CH_4} is the conversion of CH_4, S_{CO} is the selectivity of CO, F_i is the flow rate of species i, in mL·min^{-1}. F_{H_2O} can be calculated based on the hydrogen balance as follows

$$F_{CH_{4,inlet}} = F_{CH_{4,outlet}} + \frac{1}{2}F_{H_2} + \frac{1}{2}F_{H_2O} \quad (4)$$

Substitution of Eq. 3 into Eq. 4 yields

$$F_{O_{2,inlet}} = F_{O_{2,outlet}} + \frac{1}{2}F_{CO} + F_{CO_2} + F_{CH_{4,inlet}} - F_{CH_{4,outlet}} - \frac{1}{2}F_{H_2} \quad (5)$$

Results and Discussion

Materials and phase stability

Figure 3 shows the XRD patterns of the as-synthesized SCFNb and BSFM powders, which were calcined at 950°C for 5 h. XRD analysis showed the formation of perovskite structure for both samples. We exposed the powders to the atmosphere (5% H_2 + He) at 900°C to test the stability of the two kinds of materials under a reducing environment. As seen in Figure 3a, the perovskite structure of SCFNb collapses after testing for only 10 h. It is due to that Co^{3+}/Co^{4+} is vulnerable to reducing gas species.[9,53] It may also suggest that SCFNb is unsuitable under relatively high reducing atmosphere. Figure 3b shows the XRD pattern of BSFM powder. A trace amount of impurities were detected at $2\theta \approx 30°$. To our knowledge, the impurity was likely to be $BaFeO_{2.8}$ phase according to the data of PDF (Powder Diffraction File) card (54-0966). The $BaFeO_{2.8}$ phase may be attributed to the enrichment of the fast diffusivity ions at

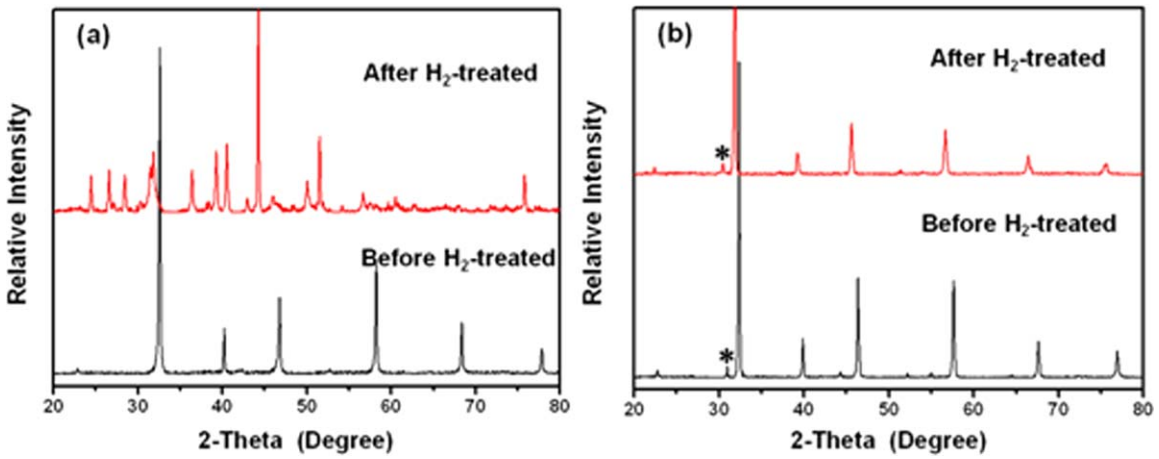

Figure 3. XRD patterns of the SCFNb and BSFM powders calcined at 950°C for 5 h, followed by annealing in a 5 vol % H_2/He atmosphere at 900°C, *: $BaFeO_{2.8}$.

(a) SCFNb H_2-treated for 10 h; (b) BSFM H_2-treated for 45 h. [Color figure can be viewed in the online issue, which is available at wileyonlinelibrary.com.]

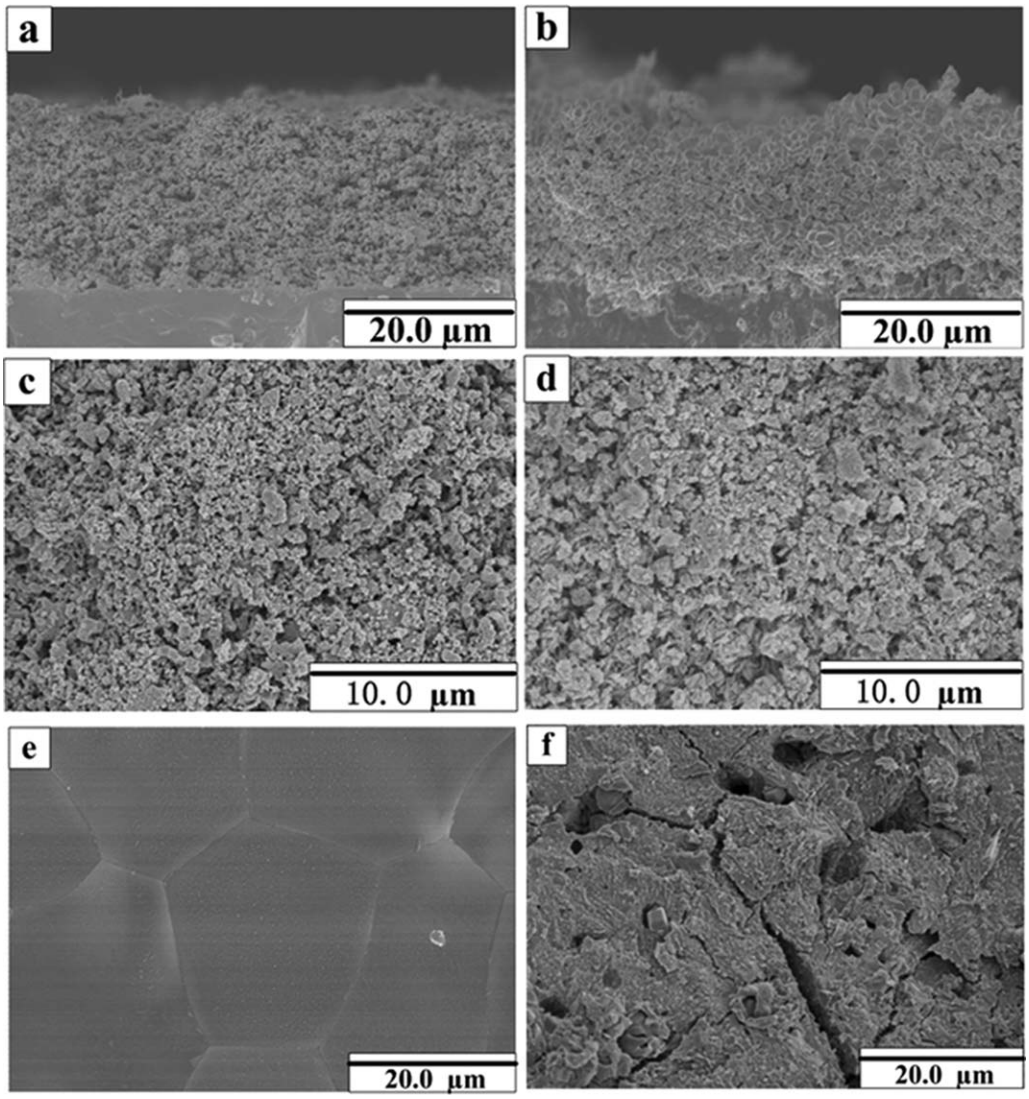

Figure 4. The SEM images of the SCFNb and BSFM-SCFNb membranes: (a) and (b) are cross sections near the reaction side of the fresh and used BSFM-SCFNb membranes.

(c) and (d) are the surface of reaction sides of the fresh and used BSFM-SCFNb membranes. (e) and (f) are the surface of the fresh and used SCFNb membranes, respectively.

grains boundaries and the external surface during sintering and subsequent heat treatment.[54] However, the amount of the impurity could be negligible. Moreover, it was noticed that the intensities of the characteristic peaks of the BSFM powder decreased a little and shifted slightly to a lower angle after reaction. It should relate to the increase in the cell parameter which results from a decrease in lattice oxygen stoichiometry in the perovskite structure during the long treatment.[55] Nevertheless, the perovskite phase still existed under such a reductive atmosphere for 45 h. We thought that BSFM oxide has high chemical stability. Similar result has been reported by Dong et al.[49]

Morphology of membranes

Figure 4 shows SEM micrographs of the SCFNb and BSFM-SCFNb dual-layer composite membranes. For the fresh SCFNb membrane, the ceramic grains with clear boundaries were visible as shown in Figure 4e. As seen in Figure 4c, the BSFM layer was porous due to the volatilization of organic solution during the heating treatment. From the cross section of BSFM-SCFNb membrane (Figure 4a), a porous layer closely adhering to a dense layer can be seen. Also, we can distinguish the porous BSFM, which approximately had a thickness of 20 μm.

BSFM-SCFNb porous-dense dual-layer composite membrane reactor

To obtain a detail performance of the BSFM-SCFNb porous-dense dual-layer composite membrane, POM was studied in the prepared disk-shape membrane reactor with Ni/Al_2O_3 catalyst. In order to clarify the performance of the porous BSFM layer, a blank experiment was carried out in a single-layer SCFNb membrane reactor without a porous BSFM layer.

Figure 5 shows the time dependence of the performance of SCFNb membrane reactor at 850°C. In this experiment, it took about 16 h to reach the steady state. Finally, CH_4 conversion of above 85%, CO selectivity of above 97%, and oxygen permeation flux of about 17 mL (STP) cm^{-2} min^{-1} were achieved for the SCFNb membrane which had a

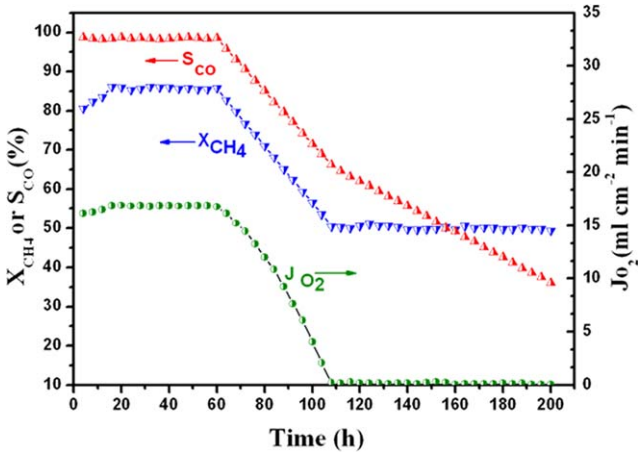

Figure 5. CO selectivity, CH_4 conversion, and O_2 permeation flux as a function of time in the SCFNb membrane reactor.

Reaction side: He = 40 mL (STP) min^{-1}, CH_4 = 5.96 mL (STP) min^{-1}; Air side: air = 100 mL (STP) min^{-1}; Temperature: 850°C. [Color figure can be viewed in the online issue, which is available at wileyonlinelibrary.com.]

thickness of 1.0 mm. It was about 11.5 times higher than that of He as the sweeping gas. This was because the permeated oxygen would quickly react with methane in reaction side, and oxygen partial pressure gradient in POM membrane reactor was much larger than that at conventional Air/He permeation condition. Unfortunately, the CH_4 conversion, CO selectivity, and oxygen permeation flux decreased extremely after about 60 h. About 100 h later, oxygen permeation flux was nearly zero and CH_4 conversion dropped to 49%. After 200 h, the CO selectivity was below 35%. Meanwhile, the concentration of N_2 detected by GC increased greatly. We deduced that the air leaked out. After stopping the reaction, we found that the SCFNb membrane cracked into several pieces. The morphology of the used SCFNb membrane surface exposed to the syngas changed after the reaction. From Figure 4f, we can see that the surface of SCFNb membrane was destroyed and became porous and loose. These results indicated that SCFNb membrane possesses a poor chemical stability to syngas production. This phenomenon also conforms well with the previous XRD patterns in Figure 3a.

The POM experiment of SCFNb membrane reactor demonstrated that the dense SCFNb ceramic membrane was unsuitable for syngas production. Thus, a BSFM-SCFNb dual-layer composite membrane in which a porous BSFM layer was coated on the surface of a dense SCFNb membrane was further investigated. In the experiment, the thickness of dense layer (SCFNb) of the dual-layer composite membrane was kept at 1.0 mm and the porous layer (BSFM) was about 20 μm.

For practical application, the membrane are operated under severely reducing environment. It was necessary to investigate the stability of BSFM-SCFNb membrane under POM reaction. Figure 6 shows the stability of the BSFM-SCFNb dual-layer composite membrane reactor at 850°C over more than 1500 h. During the period, the CO selectivity, CH_4 conversity, H_2 production, and O_2 permeation flux remained at about 97.5%, 80%, 46 mL (STP) cm^{-2} min^{-1}, 13 mL (STP) cm^{-2} min^{-1}, respectively. From the inset of Figure 6, we could see that the ratio of H_2/CO was nearly 2 and fluctuated between 1.97 and 1.99. As shown in Figure 4b, under the same reaction condition with SCFNb membrane reactor, the dense layer of BSFM-SCFNb dual-layer composite membrane still can be seen clearly and kept intact after the 1500-h POM experiment. The long-term stability testing suggests that the reduction-tolerant BSFM layer could effectively enhance the stability of SCFNb under reducing atmospheres. First, the reduction-tolerant porous BSFM layer closely adhering to the dense SCFNb layer reduced the area of bare SCFNb and avoided the direct impacting of reductive atmosphere against the SCFNb layer. Moreover, the BSFM was also a good oxygen ion conductor. The oxygen ion could partially transfer from the dense layer to the porous layer by BSFM which reduced the contact of reductive atmosphere with the dense layer.[14] Second, the good oxygen permeability of SCFNb ensured an existing of nonzero oxygen partial pressure at the surface of SCFNb layer which prevented the erosion toward the dense SCFNb layer.[47,56] The design of dual-layer porous-dense membrane reactor resulted in that the reaction site was away from the surface of dense SCFNb layer to some degree as shown in Figure 1 which prevented the direct destruction toward the SCFNb membrane effectively. Figure 4d showed that the grain size of porous BSFM layer became a little larger after the reaction. It may be because of the partial sintering of porous BSFM layer during the 1500-h operation at 850°C. The XRD patterns shown in Figure 7a indicated that the cubic perovskite structure of the both sides and the bulk of the used BSFM-SCFNb membrane still kept unchanged after the long-term operation. This result explains why the BSFM-SCFNb dual-layer composite membrane reactor could be steadily operated under the reductive atmosphere for a long run. Figure 7b showed the EDX analysis of the used membrane. We selected the unique Ba and Co elements in the porous and dense layers, respectively, for the research. As shown, the diffusion of Ba and Co elements occurred on the boundary betweeen the porous and dense layers. The diffusion depth was about 1 μm in each layer, which was not serious and could be negligible as for the performance of the

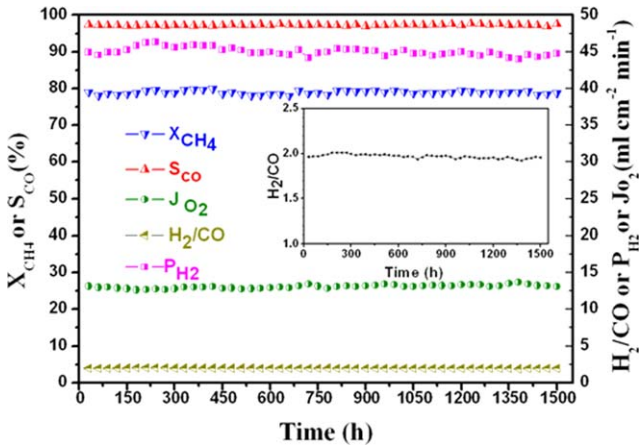

Figure 6. CO selectivity, CH_4 conversion, H_2 production, O_2 permeation flux, and H_2/CO as a function of time in the BSFM-SCFNb dual-layer composite membrane reactor.

Reaction side: He = 40 mL (STP) min^{-1}, CH_4 = 5.96 mL (STP) min^{-1}; Air side: air = 100 mL (STP) min^{-1}; Temperature: 850°C. [Color figure can be viewed in the online issue, which is available at wileyonlinelibrary.com.]

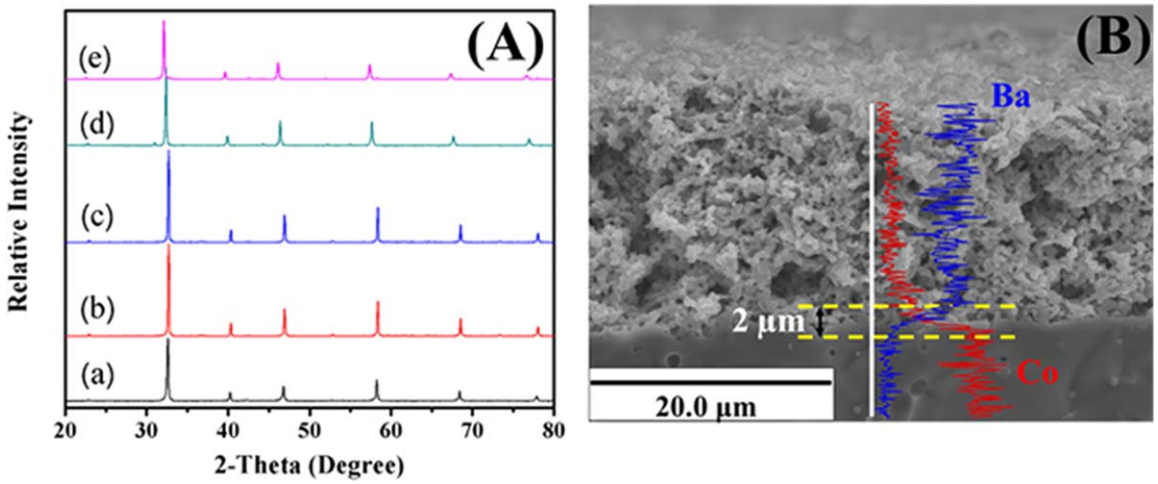

Figure 7. (a) XRD patterns of the fresh and used BSFM-SCFNb membranes: (A) and (B) are the air sides of the fresh and used BSFM-SCFNb membrane, respectively; (D) and (E) are the reaction sides of the fresh and used BSFM-SCFNb membrane, respectively; (C) bulk of the used BSFM-SCFNb membrane.

(b) EDX analysis of the used BSFM-SCFNb membrane, blue line: Ba element, red line: Co element. [Color figure can be viewed in the online issue, which is available at wileyonlinelibrary.com.]

BSFM-SCFNb membrane reactor. The oxygen permeation fluxes and stability in POM experimentals after different times are reported for various materials in Table 1. Comparing the results of BSFM-SCFNb porous-dense dual-layer composite membrane with those other membranes, we can see that the BSFM-SCFNb dual-layer composite membrane possesses a high performance in terms of the oxygen flux and the stability overall. So far, we can conclude that the BSFM-SCFNb porous-dense dual-layer composite membrane reactor was competent for POM. Meanwhile, it also showed the design of porous-dense dual-layer composite membrane reactor was successful.

Effect of operating conditions on BSFM-SCFNb dual-layer composite membrane reactor

Generally, the oxygen permeation flux, hydrogen production, CH_4 conversion, and CO selectivity are strongly affected by operating conditions such as reaction temperature, methane flow rate, air flow rate, helium flow rate, and so forth. The effects of these operating conditions on the BSFM-SCFNb porous-dense dual-layer composition membrane reactor were investigated systematically as follows.

Effect of *Temperature*. Figure 8 shows the temperature dependence of the performance of BSFM-SCFNb membrane reactor. Each temperature was held for about 1 h and the corresponding date points were recorded at least three times to ensure the accuracy of the results. Temperature has a significant effect on the membrane reaction. CH_4 conversion, hydrogen production, and oxygen permeation flux increase rapidly with increasing temperature. The increase of the oxygen permeation flux was mainly attributed to the increase in oxygen diffusion and the surface exchange kinetics with the increasing reaction temperature. For the excess feed of the CH_4, the CH_4 conversion was mainly controlled by the oxygen permeation flux. Therefore, the increase in the oxygen permeation flux spontaneously led to the increase in CH_4 conversion.[58] At 900°C, the CH_4 conversion is 99.34% and the hydrogen production is 53.67 mL (STP) cm^{-2} min^{-1}. The oxygen flux is about 18.6 mL (STP) cm^{-2} min^{-1}, which is an extraordinary value. Generally speaking, the oxygen permeation rates exceeding 15 mL (STP) cm^{-2} min^{-1} are rarely achieved. The CO selectivity increased slightly with increasing the temperature before 800°C, then decreased obviously after 850°C, and is 98.84% at 850°C. This decrease of the CO selectivity at high temperature can be explained as follows. The oxygen permeation flux increased with increasing the temperature. However, the flow rate and concentration of the feed methane was not adjusted. The CH_4/O_2 decreased at high temperatures, which led to the excessive oxidation of CO. Similar explanations were reported by many researchers in the literatures.[59,60]

Table 1. Comparison of Oxygen Fluxes and Stabilities of Various Membrane Materials in POM Experiments After Different Times

Membrane Materials	T (°C)	Thickness (mm)	O_2 Flux (mL $cm^{-2}min^{-1}$)	Time on Stream (h)	Reference
$La_{0.4}Ba_{0.6}Fe_{0.8}Zn_{0.2}O_{3-\delta}$	900	1.0	3.8	500	39
$BaCe_{0.1}Co_{0.4}Fe_{0.5}O_{3-\delta}$	875	1.0	8.9	1000	57
$BaCo_{0.7}Fe_{0.2}Nb_{0.1}O_{3-\delta}$	900	1.0	20	300	35
$Ba_{0.5}Sr_{0.5}Co_{0.8}Fe_{0.2}O_{3-\delta}$	875	1.48	11.5	500	58
$BaCo_{0.4}Fe_{0.4}Zr_{0.2}O_{3-\delta}$	850	1.0	5.6–5.8	2200	34
$BaCo_{0.7}Fe_{0.2}Ta_{0.1}O_{3-\delta}$	900	0.7	16.2	400	30
Al_2O_3-doped $SrCo_{0.8}Fe_{0.2}$ $O_{3-\delta}$	850	1.4	1.5–3.4	500	36
$SrAl_2O_4$-doped $SrCo_{0.8}Fe_{0.2}$ $O_{3-\delta}$	850	1.0	8.0	1200	37
$SrCo_{0.8}Fe_{0.2}O_{3-\delta}$	850	1.0	No date	Cracked in a short while	29
BSFM-SCFNb	850	1.0	13.0	>1500	This work

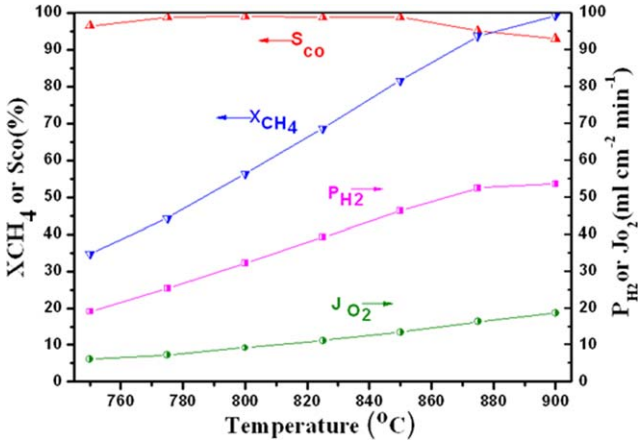

Figure 8. CO selectivity, CH_4 conversion, H_2 production, and O_2 permeation flux as a function of temperature.

He = 40 mL (STP) min^{-1}, CH_4 = 5.96 mL (STP) min^{-1}; Air side: air = 100 mL (STP) min^{-1}. [Color figure can be viewed in the online issue, which is available at wileyonlinelibrary.com.]

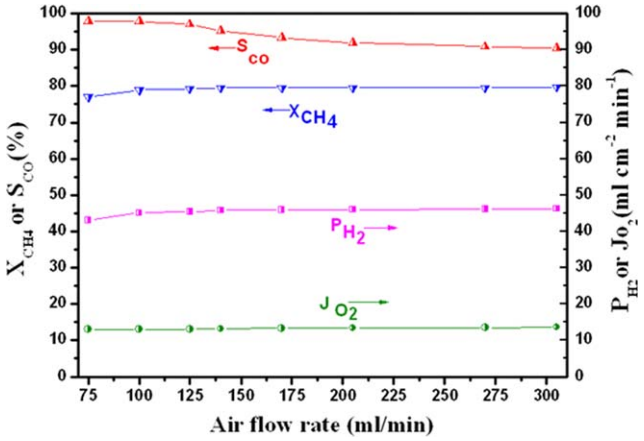

Figure 10. CO selectivity, CH_4 conversion, H_2 production, and O_2 permeation flux as a function of air flow rate.

He = 40 mL (STP) min^{-1}; CH_4 = 5.96 mL (STP) min^{-1}; Temperature: 850°C. [Color figure can be viewed in the online issue, which is available at wileyonlinelibrary.com.]

Effect of Methane Flow Rate. Figure 9 shows the methane flux dependence of oxygen permeation flux, CH_4 conversion, CO selectivity, and H_2 production when the operation temperature was unchanged at 900°C. At first, the CO selectivity, H_2 production, and oxygen permeation flux increased with increasing methane flux. On the contrary, the CH_4 conversion decreased slowly. When the CH_4 flow rate was 6.58 mL (STP) min^{-1}, the high CH_4 conversion of 97.55%, the CO selectivity of 98.67%, and the H_2 production of 60.76 mL (STP) cm^{-2} min^{-1}, the oxygen permeation flux of 18.0 mL (STP) cm^{-2} min^{-1} were achieved. With the continuous increase of the CH_4 flux, the CH_4 conversion decreased obviously. Meanwhile, the CO selectivity kept unchanged around 99% and the change of H_2 production, the oxygen permeation flux were very small. This phenomenon could be interpreted as follows. When the CH_4 flow rate was 6.58 mL (STP) min^{-1}, the CH_4/O_2 was the most suitable in terms of reaction driven force. In other words, this CH_4 concentration marked the limit the POM driven force could reach under the fixed membrane thickness and reaction temperature. After that, the oxygen permeation flux kept unchanged, and as a consequence a decrease in CH_4 conversion happened.

Effect of *Air Flow Rate*. The effect of air rate on the performance of the reaction at 850°C was shown in Figure 10. As can be seen, the influences of air flow rate on CO selectivity, CH_4 conversion, H_2 production, and O_2 permeation flux were insignificant when air flow rate is greater than 100 mL (STP) min^{-1}. This experimental finding indicates that the diffusion of air has no influence on the oxygen permeation when the air flow rate is higher than 100 mL (STP) min^{-1}. So, it is unnecessary to further increase the air flow rate when the air supplied is enough for providing stable oxygen permeation flux.

Effect of *Helium Flow Rate*. Considering the relatively low CH_4 conversion during the long-term operation, we

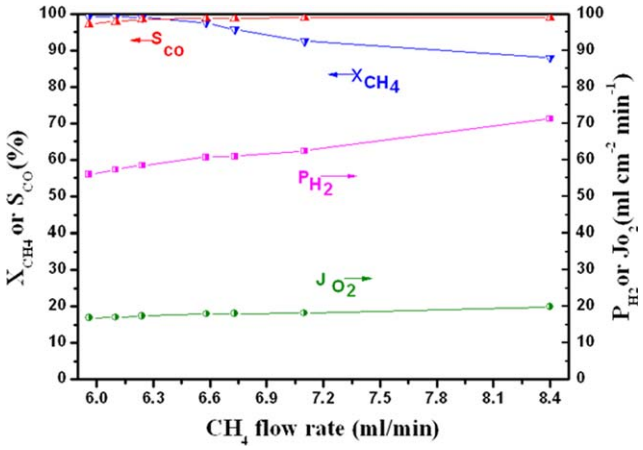

Figure 9. CO selectivity, CH_4 conversion, H_2 production, and O_2 permeation flux as a function of CH_4 flux.

He = 40 mL (STP) min^{-1}; Air side: air = 100 mL (STP) min^{-1}; Temperature: 900°C. [Color figure can be viewed in the online issue, which is available at wileyonlinelibrary.com.]

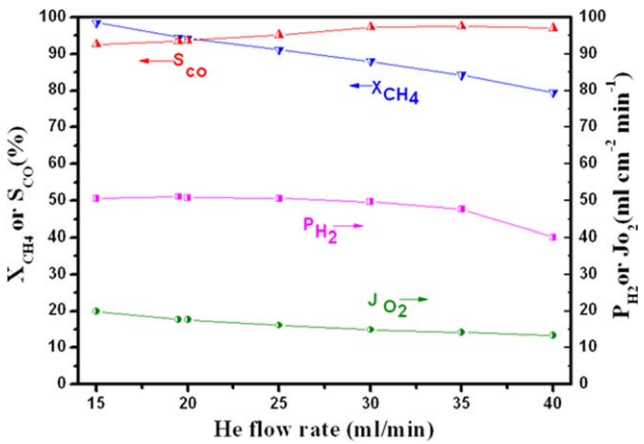

Figure 11. CO selectivity, CH_4 conversion, H_2 production, and O_2 permeation flux as a function of He flow rate.

Reaction side: CH_4 = 5.96 mL (STP) min^{-1}; Air side: air = 100 mL (STP) min^{-1}; Temperature: 850°C. [Color figure can be viewed in the online issue, which is available at wileyonlinelibrary.com.]

intentionally studied the impact of the methane partial pressure on the CH_4 conversion. In the experiment, we changed the methane partial pressure by fixing the flow rate of CH_4 and changing the flow rate of He. As shown in Figure 11, the CH_4 conversion increased from 79.4 to 98.6% rapidly with decreasing the flow rate of He from 40 to 15 mL (STP) min^{-1}. Therefore, the experimental parameters of POM in BSFM-SCFNb dual-layer composite membrane need to be further optimized next. The increase of CH_4 conversion can be explained as follow. The decrease of the He flow rate would result in an increase in the CH_4 partial pressure in the reactive side. The increase of CH_4 partial pressure increased the oxygen flux, and then the CH_4 conversion. Gu et al.[61] also reported that oxygen flux increased with increasing the methane partial pressure.

The performance of the BSFM-SCFNb porous-dense dual-layer composite membrane reactor made changes regularly under different conditions. It is convenient for us to find the suitable condition with specific applications. It is noticed that the porous-dense dual-layer composite membrane reactor survived from the testing under different conditions. This fully showed that the dual-layer composite membrane reactor had a sufficient stability.

Conclusions

We designed a BSFM-SCFNb porous-dense dual-layer composite membrane reactor. POM was conducted in the membrane reactor to confirm the feasibility of the porous-dense dual-layer design philosophy. The stability of the SCFNb membrane was largely improved by the porous BSFM layer on the reaction side. The maximum oxygen permeation flux reached 18.6 mL (STP) cm^{-2} min^{-1} in the BSFM-SCFNb dual-layer composite membrane at 900°C, which is a high value under the POM condition among the membrane reported in the literature. At the same time, 99.34% CH_4 conversion, 94% CO selectivity, and a hydrogen production of 53.67 mL (STP) cm^{-2} min^{-1} have been achieved at 900°C. The porous-dense BSFM-SCFNb dual-layer composite membrane reactor was operated stably for more than 1500 without any degradation of reaction performance. SEM characterization of the used BSFM-SCFNb dual-layer composite membrane hardly showed any change. The dense layer of the BSFM-SCFNb dual-layer composite membrane still kept intact as well. The membrane could survive the long-term operation that showed a potential application for syngas or hydrogen production by POM. Also, the design of porous-dense dual-layer composite membrane reactor can be regarded as a good candidate for acquiring the balance between high oxygen permeability and sufficient chemical stability with MIEC membrane reactor when used for potential industrial applications.

Acknowledgments

This work was supported by the National Basic Research Program of China (No. 2009CB623406); National Natural Science Foundation of China (No. 20990222, No. 21006047); China Postdoctoral Science Foundation (No. 20090461105, No. 201003581).

Literature Cited

1. Dalmon JA, Giroir-Fendler A, Mirodatos C, Mozzanega H. Proceedings of the first international workshop on catalytic membranes-Lyon–Villeurbanne, France, September 26–28, 1994-Foreword. *Catal Today*. 1995;25:197–197.
2. Sanchez Marcano JG, Tsotsis TT. Catalytic Membranes and Membrane Reactors. Weinhein: Wiley-VCH Verlag GmbH, 2002.
3. Drioli E, Paul DR. Preface: Advanced membrane technology III: Membrane engineering for process intensification conference. *Ind Eng Chem Res*. 2007;46:2235.
4. Sale DA, Dyncan AM, Nordheden KJ, Stagg-Williams SM. Mixed-conducting oxygen permeable ceramic membranes for the carbon dioxide reforming of methane. *Green Chem*. 2007;9:577–581.
5. Tsai CY, Dixon AG, Moser WR, Ma YH. Dense perovskite membrane reactors for partial oxidation of methane to syngas. *AIChE J*. 1997;43:2741–2750.
6. Zhu XF, Wang HH, Cong Y, Yang WS. Partial oxidation of methane to syngas in $BaCe_{0.15}Fe_{0.85}O_{3-\delta}$ membrane reactors. *Catal Lett*. 2006;111:179–185.
7. Wang HH, Tabet C, Schiestel T, Werth S, Caro J. Partial oxidation of methane to syngas in a perovskite hollow fiber membrane reactor. *Catal Commun*. 2006;7:907–912.
8. Jin WQ, Li SG, Huang P, Xu NP, Shi J, Lin YS. Tubular lanthanum cobaltite-type membrane reactor for partial oxidation of methane to syngas. *J Memb Sci*. 2000;166:13–22.
9. Bouwmeester HJW. Dense ceramic membranes for methane conversion. *Catal Today*. 2003;82:141–150.
10. Tan XY, Li K. Design of mixed conducting ceramic membrane/reactors for the partial oxidation of methane to syngas. *AIChE J*. 2009; 55:2675–2685.
11. Jin WQ, Zhang C, Zhang P, Fan YQ, Xu NP. Thermal decomposition of carbon dioxide coupled with POM in a membrane rector. *AIChE J*. 2006;52:2545–2550.
12. Kniep J, Lin YS. Partial oxidation of methane and oxygen permeation in $SrCoFeO_X$ membrane reactors with different catalysts. *Ind Eng Chem Res*. 2011;50:7941–7948.
13. Cheng HW, Liu JZ, Lu XG, Ding WZ. Enhancing the oxygen permeability of $BaCo_{0.7}Fe_{0.2}Nb_{0.1}O_{3-\delta}$ membranes by coating $GdBaCo_{2-x}Fe_xO_{5+\delta}$ for partial oxidation of coke oven gas to syngas. *Appl Mater Interfaces*. 2011;3:4032–4039.
14. Dong XL, Zhang C, Chang XF, Jin WQ, Xu NP. A self-catalytic membrane reactor based on a supported mixed-conducting membrane. *AIChE J*. 2008;54:1678–1680.
15. Zhang YW, Liu JA, Ding WZ, Lu XG. Performance of an oxygen-permeable membrane reactor for partial oxidation of methane in coke oven gas to syngas. *Fuel*. 2011;90:324–330.
16. Balachandran U, Lee TH, Dorris SE. Hydrogen production by water dissociation using mixed conducting dense ceramic membranes. *Int J Hydrogen Energy*. 2007;32:451–456.
17. Mundschau MV, Xie X, Evenson CR IV, Sammells AF. Dense inorganic membranes for production of hydrogen from methane and coal with carbon dioxide sequestration. *Catal Today*. 2006;118:12–23.
18. Zhu N, Dong XL, Liu ZK, Zhang GR, Jin WQ, Xu NP. Toward highly-effective and sustainable hydrogen production: bio-ethanol oxidative steam reforming coupled with water splitting in a tubular membrane reactor. *Chem Commun*. 2012;48:7137–7139.
19. Akin FT, Lin YS. Selective oxidation of ethane to ethylene in a dense tubular membrane reactor. *J Memb Sci*. 2002;209:457–467.
20. Akin FT, Lin YS. Oxidative coupling methane in dense ceramic membrane reactor with high yields. *AIChE J*. 2002;48:2298–2306.
21. Czuprat O, Werth S, Caro J, Schiestel T. Oxidative dehydrogenation of propane in a perovskite membrane reactor with multi-step oxygen insertion. *AIChE J*. 2010;56:2390–2396.
22. Tan XY, Li K. Oxidative coupling of methane in a perovskite hollow-fiber membrane reactor. *Ind Eng Chem Res*. 2006;45:142–149.
23. Jin WQ, Zhang C, Chang XF, Fan YQ, Xing WH, Xu NP. Efficient catalytic decomposition of CO_2 to CO and O_2 over Pd/mixed-conducting oxide catalyst in an oxygen-permeable membrane reactor. *Environ Sci Technol*. 2008;42:3064–3068.
24. Jiang HQ, Xing L, Czuprat O, Wang HH, Schirrmeister S, Schiesteld T, Caro J. Highly effective NO decomposition by in situ removal of inhibitor oxygen using an oxygen transporting membrane. *Chem Commun*. 2009;44:6738–6740.
25. Jiang HQ, Wang HH, Liang FY, Werth S, Caro J. Direct decomposition of nitrous oxide to nitrogen by in situ oxygen removal with a perovskite membrane. *Angew Chem Int Ed*. 2009;48:2983–2986.
26. Li K. Ceramic Membranes for Separation and Reaction. England: Wiley, 2007.

27. Zhang C, Chang XF, Dong XL, Jin WQ, Xu NP. The oxidative stream reforming of methane to syngas in a thin tubular mixed-conducting membrane reactor. *J Memb Sci*. 2008;320:401–406.
28. Sunarso J, Baumann S, Serra JM, Meulenberg WA, Liu S, Lin YS, Diniz da Costa JC. Mixed ionic-electronic conducting (MIEC) ceramic-based membranes for oxygen separation. *J Memb Sci*. 2008; 320:13–41.
29. Pei S, Kleefisch MS, Kobylinski TP, Faber J, Udovich CA. Failure mechanisms of ceramic membrane reactors in partial oxidation of methane to synthesis gas. *Catal Lett*. 1995;30:201–212.
30. Luo HX, Wei YY, Jiang HQ, Yuan WH, Lv YX, Caro J, Wang HH. Performance of a ceramic membrane reactor with high oxygen flux Ta-containing perovskite for the partial oxidation of methane to syngas. *J Memb Sci*. 2010;350:154–160.
31. Jiang HQ, Cao ZW, Schirrmeister S, Schiestel T, Caro J. A coupling strategy to produce hydrogen and ethylene in a membrane reactor. *Angew Chem Int Ed*. 2010;49:5656–5660.
32. Ishihara T, Yamada T, Arikawa H, Nishiguchi H, Takita Y. Fe doped $LaGaO_3$ perovskite oxide as an oxygen separating membrane for CH_4 partial oxidation. *Solid State Ionics*. 2002;152:709–714.
33. Shaula AL, Kharton VV, Marques FMB. Ionic and electronic conductivities, stability and thermal expansion of $La_{10-x}(Si, Al)_{(6)}O_{26\pm\delta}$ solid electrolytes. *Solid State Ionics*. 2006;177:1725–1728.
34. Tong JH, Yang WS, Cai R, Zhu BC, Lin LW. Novel and ideal zirconium-based dense membrane reactors for partial oxidation of methane to syngas. *Catal Lett*. 2002;78:129–137.
35. Makoto H, Kazunari D, Michhikazu D, Takashi T. $Ba_{1.0}Co_{0.7}Fe_{0.2}Nb_{0.1}O_{3-\delta}$ dense ceramic as an oxygen permeable membrane for partial oxidation of methane to synthesis gas. *Chem Lett*. 2006;35: 1326–1327.
36. Wu ZT, Jin WQ, Xu NP. Oxygen permeability and stability of Al_2O_3-doped $SrCo_{0.8}Fe_{0.2}O_{3-\delta}$ mixed conducting oxides. *J Memb Sci*. 2006;279:320–327.
37. Dong XL, Liu ZK, He YJ, Jin WQ, Xu NP. $SrAl_2O_4$-improved $SrCo_{0.8}Fe_{0.2}O_{3-\delta}$ mixed-conducting membrane for effective production of hydrogen from methane. *J Memb Sci*. 2009;331:109–116.
38. Kharton VV, Waerenborgh JC, Rojas DP, Yaremchenko AA, Valente AA, Shaula AL, Patrakeev MV, Marques FMB, Rocha J. Mossbauer spectra and catalytic behavior of perovskite-like $SrFe_{0.7}Al_{0.3}O_{3-\delta}$. *Catal Lett*. 2005;99:249–255.
39. Gong ZL, Hong L. Integration of air separation and partial oxidation of methane in the $La_{0.4}Ba_{0.6}Fe_{0.8}Zn_{0.2}O_{3-\delta}$ membrane reactor. *J Memb Sci*. 2011;380:81–86.
40. Zhu XF, Liu HY, Cong Y, Yang WS. Novel dual-phase membranes for CO_2 capture via an oxyfuel route. *Chem Commun*. 2012;48:251–253.
41. Luo HX, Jiang HQ, Klande T, Cao ZW, Liang FY, Wang HH, Caro J. Novel cobalt-free, noble metal-free oxygen-permeable $40Pr_{0.6}Sr_{0.4}FeO_{3-\delta}-60Ce_{0.9}Pr_{0.1}O_{2-\delta}$ dual-phase membrane. *Chem Mater*. 2012;24:2148−2154.
42. Luo YL, Liu T, Gao JF, Chen CS. $Zr_{0.84}Y_{0.16}O_{1.92}$-$La_{0.8}Sr_{0.2}Cr_{0.5}Fe_{0.5}O_{3-\delta}$ composite membrane for CO_2 decomposition. *Mater Lett*. 2012;86:5–8.
43. Zhu XF, Li QM, Cong Y, Yang WS. Syngas generation in a membrane reactor with a highly stable ceramic composite membrane. *Catal Commun*. 2008;10:309–312.
44. Bredesen R, Sogge J. Paper Presented at the United Nations Economic Commission for Europe Seminar on Ecological Applications of Innovative Membrane Technology in Chemical Industry, Chem/Sem. 21/R.12, Cetaro, Calabria, Italy, May 1–4, 1996.
45. Zhang C, Chang XF, Fan YQ, Jin WQ, Xu NP. Improving performance of a dense membrane reactor for thermal decomposition of CO_2 via surface modification. *Ind Eng Chem Res*. 2007;46:2000–2005.
46. Zhang C, Jin WQ, Yang C, Xu NP. Decomposition of CO_2 coupled with POM in a thin tubular oxygen-permeable membrane reactor. *Catal Today*. 2009;148:298–302.
47. Chang XF, Zhang C, He YJ, Dong XL, Jin WQ, Xu NP. A comparative study of the performance of symmetric and asymmetric mixed-conducting membranes. *Chin J Chem Eng*. 2009;17:562–570.
48. Zhang GR, Liu ZK, Zhu N, Jiang W, Dong XL, Jin WQ. A novel Nb_2O_5-doped $SrCo_{0.8}Fe_{0.2}O_{3-\delta}$ oxide with high permeability and stability for oxygen separation. *J Memb Sci*. 2012;405–406:300–309.
49. Dong XL, Jin WQ, Xu NP. Reduction-tolerant oxygen-permeable-type oxide $Sr_{0.7}Ba_{0.3}Fe_{0.9}Mo_{0.1}O_{3-\delta}$. *Chem Mater*. 2010;22:3610–3618.
50. Liu ZK, Zhang GR, Dong XL, Jiang W, Jin WQ, Xu NP. Fabrication of asymmetric tubular mixed-conducting dense membranes by a spin-spraying and co-sintering process. *J Memb Sci*. 2012;415–416:313–319.
51. Kontoulis I, Steele BCH. Determination of oxygen diffusion in solid Ag by an electrochemical technology. *Solid State Ionics*. 1991;47: 317–324.
52. Lee TH, Yang YL, Jacobson AJ. Electrical conductivity and oxygen permeation of Ag/BaBi8O13 composites. *Solid State Ionics*. 2000; 134:331–339.
53. Konysheva E, Irvine JTS. Thermochemical and structural stability of A- and B site-substituted perovskites in hydrogen-containing atmosphere. *Chem Mater*. 2009;21:1514–1523.
54. Bouwmeester HJW, Burggraaf AJ. Dense ceramic membranes for oxygen separation. In: Burggraaf AJ, Johnson DH, editors. *Fundamentals of Inorganic Membrane Science and Technology*. Amsterdam: Elsevier B V, 1996:435–528.
55. Marina OA, Canfield NL, Stevenson JW. Thermal, electrical, and electrocatalytical properties of lanthanum-doped strontium titanate. *Solid State Ionics*. 2002;149:21–28.
56. Wang HH, Feldhoff A, Caro J, Schiestel T, Werth S. Oxygen selective ceramic hollow fiber membranes for partial oxidation of methane. *AIChE J*. 2009;55:2657–2664.
57. Li QM, Zhu XF, He YF, Yang WS. Partial oxidation of methane in $BaCe_{0.1}Co_{0.4}Fe_{0.5}O_{3-\delta}$ membrane reactor. *Catal Today*. 2010;149: 185–190.
58. Dong H, Shao ZP, Xiong GX, Tong JH, Sheng SS, Yang WS. Investigation on POM reaction in a new perovskite membrane reactor. *Catal Today*. 2001;67:3–13.
59. Ikeguchi M, Mimura T, Sekine Y, Kikuchi E, Matsukata M. Reaction and oxygen permeation studies in $Sm_{0.4}Ba_{0.6}Fe_{0.8}Co_{0.2}O_{3-\delta}$ membrane reactor for partial oxidation of methane to syngas. *Appl Catal A Gen*. 2005;290:212–220.
60. Bayraktar D, Clemens F, Diethelm S, Graule T, Van herle J, Holtappels P. Production and properties of substituted $LaFeO_3$-perovskite tubular membranes for partial oxidation of methane to syngas. *J Eur Ceram Soc*. 2007;27:2455–2461.
61. Gu XH, Jin WQ, Chen CL, Xu NP, Shi J. YSZ-$SrCo_{0.4}Fe_{0.6}O_{3-\delta}$ membrane for the partial oxidation of methane to syngas. *AIChE J*. 2002;48:2051–2060.

Manuscript received Feb. 3, 2013, and revision received Apr. 27, 2013.